Heat Budget of Tropical Ocean and Atmosphere[1]

STEFAN HASTENRATH

Department of Meteorology, University of Wisconsin, Madison 53706

(Manuscript received 14 March 1979, in final form 10 September 1979)

ABSTRACT

Heat budget estimates for the global tropics are derived from recent calculations of the oceanic heat budget and satellite measurements of net radiation at the top of the atmosphere. Annual mean heat export from the zone 30°N–30°S amounts to $\sim 101 \times 10^{14}$ W (=100 units). Of this total 39 and 61 units are performed within the oceanic water body and the atmospheric column over sea and land, respectively. In the zone 0–10°N, to which the planetary cloud band (ITCZ) is essentially limited throughout the year, atmospheric heat export reaches only 13 units, as compared to an oceanic export of 18 units from the zone 0–10°S. In particular, oceanic export in the belt 0–5°S alone contributes 11 units which is 90% of the net radiative heat gain at the top of the atmosphere in this latitude zone. Accordingly, the atmospheric heat export from the realm of the ITCZ related to hot tower mechanisms seems to play a more modest *relative* role in the global heat budget than heretofore believed. By comparison, oceanic export from the cold water zones immediately to the south of the Atlantic and Pacific equator emerges as an important factor in global energetics.

Oceanic meridional heat transport in the Pacific is directed from the tropics into either hemisphere; in the Atlantic it is northward from high southern latitudes all the way to the arctic; and it is directed southward in the Indian Ocean. Oceanic heat gain in the Pacific offsets deficits in the higher southern latitudes of the Atlantic and Indian Ocean sectors, as well as in the Atlantic as a whole. Meridional heat transport for all oceans combined is largest around 30°N and 25°S, where it accounts for 53 and 35% of the total poleward transport. Atmospheric transport is largest and effects the bulk of the total transport in midlatitudes.

Appreciably different estimates of net radiation at the top of the atmosphere, and of oceanic and atmospheric heat export must be regarded as compatible within the broad error limits indicated at present for all three terms.

1. Introduction

Net radiation at the upper boundary of the earth amounts to a heat gain in the tropics and a loss in higher latitudes. Redistribution of energy over the continents takes place exclusively in the atmosphere, whereas in the realm of the vast tropical oceans both atmosphere and hydrosphere cooperate in the heat export to other parts of the globe. The partitioning of atmospheric versus oceanic heat transports is of fundamental interest in global energetics. Quantitative estimates of this breakdown have been obtained for the Atlantic, Pacific and Indian Oceans (Hastenrath, 1977a,b; Hastenrath and Lamb, 1980), based on satellite measurements of net radiation at the top of the atmosphere and computations of the oceanic heat budget that have recently become available. The present paper examines the relative role of atmospheric and oceanic exports for the tropics at large.

2. Data

The heat budget of the Atlantic and Indian Oceans has been calculated recently on the basis of long-term ship observations. For the period 1911–70, more than 7 million observations over the tropical Atlantic and eastern Pacific Oceans, and about 4.5 million observations over the Indian Ocean, were available. These data were obtained in the form of individual monthly means from the National Climatic Center, Asheville, NC. Each observation includes several parameters, such as sea level pressure, wind direction and speed, sea surface and air temperature, dew point, total cloudiness, etc. Data have been evaluated in atlases of climate and circulation, and of the oceanic heat budget, with a 1° square spatial resolution (Hastenrath and Lamb, 1977, 1978b, 1979). Details of data and computational procedures are discussed in these publications.

Data for the oceanic heat budget of the Pacific are available from Wyrtki's (1965) study. The spatial resolution of his charts warrants an evaluation by 5° square areas. Budyko's (1963) data extend Wyrtki's (1965) mapping to the 20–30°S zone.

Satellite-derived net radiation data for the top of the atmosphere over a few years have been published recently (Vonder Haar and Ellis, 1974; Oort and Vonder Haar, 1976; Gruber, 1978), but these refer to the middle of 10° squares or entire latitude belts.

[1] Dedicated to Professor Heinz Lettau for his 70th birthday.

0022-3670/80/020159-12$07.00

TABLE 1. Annual mean net radiation at the top of the atmosphere SWLW$\Uparrow_{top}$ (W m^{-2}). For the continents, numbers not in parentheses are computed from 10° squares lying within area of dense dot roster in Fig. 1; values computed from areas that include blocks with sparse pattern are given in parentheses.

Latitude zone	Pacific	Atlantic	Indian	Americas	Africa	South Asia	Australia
30–20°N	+24	+35	—	(+35)	−7	+13 (+11)	—
20–10°N	+51	+54	+56	(+52)	+32	(+49)	—
10–0°N	+65	+72	+78	(+59)	+65	(+70)	—
0–10°S	+61	+66	+78	+54	+63	(+63)	—
10–20°S	+48	+52	+61	+42	+45	—	(+47)
20–30°S	+37	+36	+34	+35	+21	—	+21

Areas evaluated and referred to in Table 1 and Figs. 5–9 are explained in Fig. 1. Fig. 2 permits a comparison with the position of major cloud bands and the characteristics of the sea surface temperature patterns during the extreme seasons.

3. Basic theory

The present section is in part repeated from Hastenrath (1977a). A heat budget scheme for the atmosphere-ocean-land system is illustrated in Fig. 3. The budget equation for the system can be written

$$\text{SWLW}\Uparrow_{\text{top}} = Q_{va} + Q_{ta} + Q_{vo} + Q_{to}. \quad (1)$$

The left-hand term signifies the net radiation at the top of the atmosphere; in the right-hand terms, the subscripts v and t denote divergence of heat transport and storage, respectively, and the subscripts a and o refer to atmosphere and ocean-land.

For the long-term mean annual conditions considered here, the second and fourth right-hand terms of Eq. (1) vanish. Moreover, for land areas the third right-hand term does not arise, and hence $\text{SWLW}\Uparrow_{\text{top, land}} = Q_{va,\text{ land}}$. On the other hand, for ocean areas, $\text{SWLW}\Uparrow_{\text{top, ocean}} = Q_{va,\text{ ocean}} + Q_{vo}$.

The heat budget equation for the atmospheric column reads

$$Q_{va} + Q_{ta} = [\text{SWLW}\Uparrow_{\text{top}} - \text{SWLW}\Uparrow_{\text{sfc}}] + Q_e + Q_s, \quad (2)$$

where the right-hand terms denote the net radiative cooling of the atmospheric column, and latent and sensible heat transfer at the ocean and/or land surface, respectively.

When the atmospheric heat export is evaluated directly, separate budget equations are used for geopotential energy and sensible heat ($gz + c_pT$) and for latent heat, respectively (Riehl and Malkus, 1958; Hastenrath, 1966; Hastenrath and Lamb, 1980); the contribution of kinetic energy $V^2/2$ is small by comparison. Adding those two equations yields Eq. (2). However, the data described in Section 2 do not warrant a separate consideration of the various forms of atmospheric energy.

For the heat budget of ocean-land

$$\text{SWLW}\Uparrow_{\text{sfc}} = Q_e + Q_s + Q_{vo} + Q_{to}, \quad (3)$$

the left-hand term being the net radiation at the ocean and/or land surface. The third right-hand term is zero for land surfaces as in Eq. (1). Likewise, the terms Q_{to} and Q_{ta} in Eqs. (2) and (3) vanish as in Eq. (1) for the long-term mean annual conditions considered here.

4. Patterns of planetary net radiation and oceanic and atmospheric heat export

The annual mean patterns of net radiation at the top of the atmosphere, and of heat export within ocean and atmosphere, are mapped in Fig. 4, and

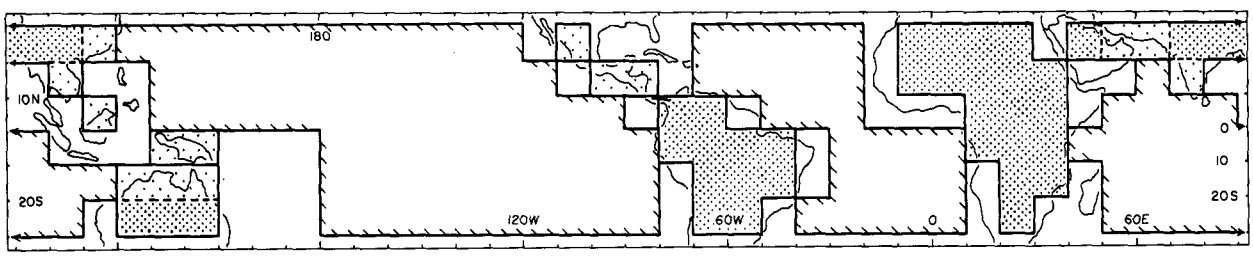

FIG. 1. Orientation map. Boxes denote areas for which heat budget data were evaluated. Blocks delineated by cross-hatching are ocean areas, and dot roster blocks mark land areas referred to in Fig. 5 and Table 1; dense dot pattern pertains to 10° squares limited nearly completely to land. The entire continents and oceans, from coast to coast, are referred to in Tables 2, 3 and Figs. 7–11, with 120°E being chosen as boundary between the Pacific and Indian Oceans. In Fig. 6 the entire ocean area is used, but for the Pacific the western boundary is as indicated in Fig. 1.

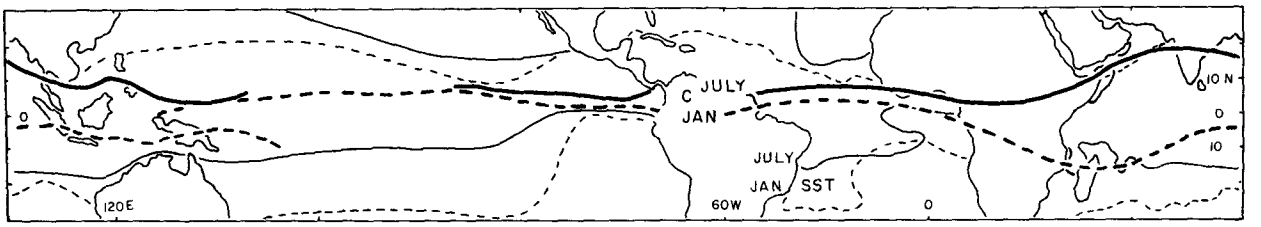

FIG. 2. Major cloud bands (heavy line) and 25°C isotherm of sea surface temperature (thin lines) during January (broken) and July (solid). Cloud information is taken from Atkinson and Sadler (1970), and sea surface temperature data from Hastenrath and Lamb (1979) for the Indian Ocean, from Hastenrath and Lamb (1977) for the Atlantic, and from U.S. Navy Hydrographic Office (1944) and Hastenrath and Lamb (1977) for the Pacific Ocean.

mean meridional profiles are shown in Figs. 5–8 and Tables 1 and 3–5.

Fig. 4a, constructed from data by Vonder Haar and Ellis (1974), shows a heat gain for the entire map area except the deserts of northern Africa, largest amounts in the equatorial belt, and a decrease toward the subtropics. Spatial details, such as the maxima in the northern equatorial Pacific and Atlantic, the northwest to southeast orientation of isopleths over South America, and the smaller values to the north as compared to the south of the equator in Africa, are broadly consistent with the cloudiness pattern (Atkinson and Sadler, 1970). These features are reflected in hemispheric asymmetries over the individual oceans and continents (Table 1), which are further apparent in the meridional profiles for all oceans and all continents combined, respectively (Fig. 5). Values tend to be smaller over the continents, as a result of larger cloudiness.

The map of mean annual heat gain by the oceanic water body (Fig. 4b) is based on Hastenrath and Lamb (1978b, 1979) for the Atlantic and Indian Oceans, and on Wyrtki (1966) and Budyko (1963), respectively, for latitudes 30°N–20°S and 20–30°S in the Pacific. For the areas of overlap, Wyrtki's (1966) values differ from those of Hastenrath and Lamb (1978b) toward larger oceanic heat gain. The map shows heat export for much of the low-latitude oceans, but especially so for the cold water regions immediately to the south of the equator in the Atlantic and the eastern and central Pacific, as well as off the west coasts of southern and northern Africa and South America (Fig. 2). Import is indicated for much of the southern subtropical oceans, the warm current regions of the western North Atlantic, and the westernmost North Pacific. Import or relatively small export is also characteristic of the regions of zonally oriented cloud bands (Fig. 2) immediately to the north of the Atlantic and eastern Pacific Equator.

Mean meridional profiles for the three oceans are depicted in Fig. 6. Both the Atlantic and Pacific show the major maximum of Q_{vo} in the latitude band immediately to the south of the equator. Export is indicated for most latitude bands. The Indian Ocean shows a contrastingly different pattern in that export, i.e., positive Q_{vo}, is largest in the northern Indian Ocean, decreases southward, and changes to import in the outer tropics of the Southern Hemisphere. The most remarkable feature in the latitudinal distribution of Q_{vo} for all oceans combined (Figs. 5, 7 and 8) is the hemispheric asymmetry with a prominent maximum to the south of the equator. Thus the meridional pattern for the tropical hydrosphere as a whole is dominated by the Pacific and Atlantic Oceans.

A major cause for the differing meridional heat budget patterns in the various oceans can be appreciated from the profiles of sea surface temperature plotted in Fig. 6. In the Atlantic and Pacific, the zone immediately to the South is much colder

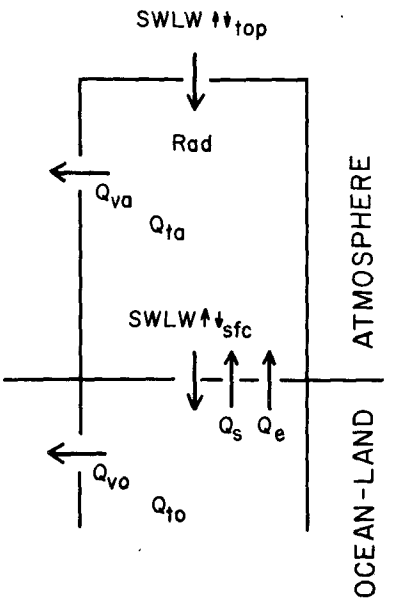

FIG. 3. Heat budget scheme for atmosphere-ocean-land system. SWLW $\Uparrow\Downarrow_{top}$ and SWLW $\Uparrow\Downarrow_{sfc}$ denote net radiation at the top of the atmosphere and at the ocean and land surface, respectively; Rad = SWLW $\Uparrow\Downarrow_{top}$ − SWLW $\Uparrow\Downarrow_{sfc}$; Q_v is divergence of horizontal heat transport, Q_t storage; subscripts a and o refer to atmosphere and ocean–land; and Q_s and Q_e refer to sensible and latent heat flux at the surface.

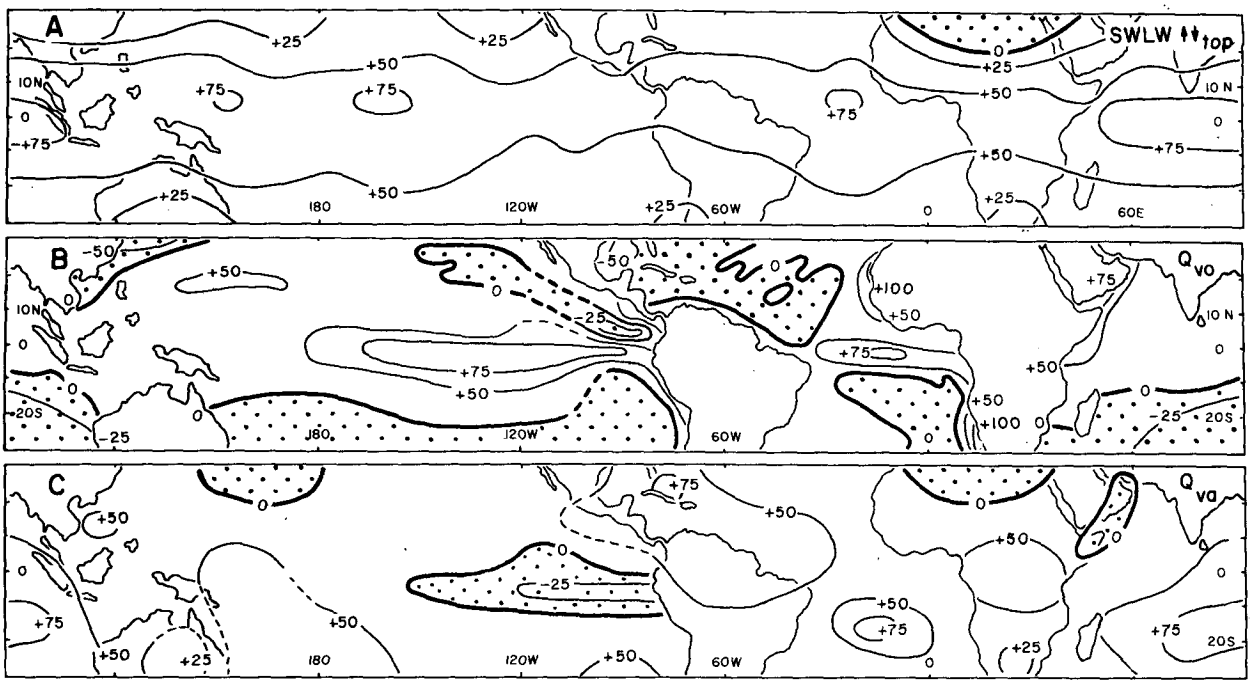

FIG. 4. Annual mean maps of heat budget components (W m^{-2}). (a) Net radiation at the top of the atmosphere SWLW ⇅ (source: Vonder Haar and Ellis, 1974). (b) Heat export (positive) within the ocean Q_{vo} [sources: Hastenrath and Lamb (1980) for the Indian Ocean; Hastenrath and Lamb (1978) for the Atlantic; Wyrtki (1966), Hastenrath and Lamb (1978) and Budyko (1963) for the Pacific]. (c) Heat export (positive) within the atmosphere, Q_{va} (sources: as in 4a and 4b). Spatial resolution corresponds to 5° squares for (b), and to 10° squares for (a) and (c). In (b) and (c) isopleths of 25 and 75 are drawn at extrema only, and interpolated isopleths are denoted by broken lines. Negative areas are shown by dot raster.

than the band to the north of the equator (Figs. 2 and 6). This is a feature of the eastern Atlantic and Pacific in particular (Hastenrath, 1978; Hastenrath and Lamb, 1977, 1979; Wyrtki, 1966; U.S. Navy Hydrographic Office, 1944). These are also regions

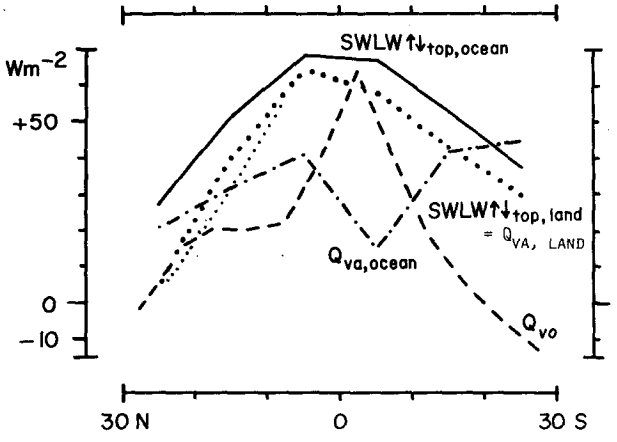

FIG. 5. Annual mean meridional profiles for the oceanic and continental portions of the global tropics. Net radiation at the top of the atmosphere over the ocean, SWLW $\Uparrow\Downarrow_{top,\,ocean}$, is denoted by solid, and over land, SWLW $\Uparrow\Downarrow_{top,\,land}$ $(= Q_{va,\,land})$, by dotted line; thin dotted line refers to 10° blocks designated by dense dot raster in Fig. 1. Heat export within the ocean, Q_{vo}, is shown as a broken line and residual heat export within the atmosphere, $Q_{va,\,ocean}$ as dash-dotted (source: Fig. 4).

of rather small sensible and latent heat transfer (Hastenrath, 1978; Hastenrath and Lamb 1978b, 1979; Wyrtki, 1966). In the Indian Ocean, the sensible and latent heat flux increases from the Northern toward the Southern Hemisphere, without a minimum near the equator (Hastenrath and Lamb, 1979, 1980). A near-equatorial minimum of sea surface temperature is likewise lacking. This examination shows that the prominent maximum of Q_{vo} immediately to the south of the equator, which characterizes the tropical hydrosphere as a whole (Figs. 5, 7 and 8), results from the contribution of the reduced heat transfer in the cold water tongues of the eastern Atlantic and Pacific Oceans in particular. The cold water surface is conducive to small latent and sensible heat expenditures and hence a large oceanic energy gain. However, the latter is not used locally to raise the sea surface temperature, as a result of the hydrospheric vertical motion pattern, which in turn is related to the dynamics of the coupled ocean-atmosphere system (Hastenrath, 1978; Hastenrath and Lamb, 1978a).

The map of heat export within the atmosphere Q_{va} (Fig. 4c) is the difference between the patterns of net radiation at the top of the atmosphere SWLW $\Uparrow\Downarrow_{top}$ and oceanic heat export Q_{vo} depicted in Figs. 4a and 4b, respectively. Data for the latter quantity are available by 5° square areas, but for

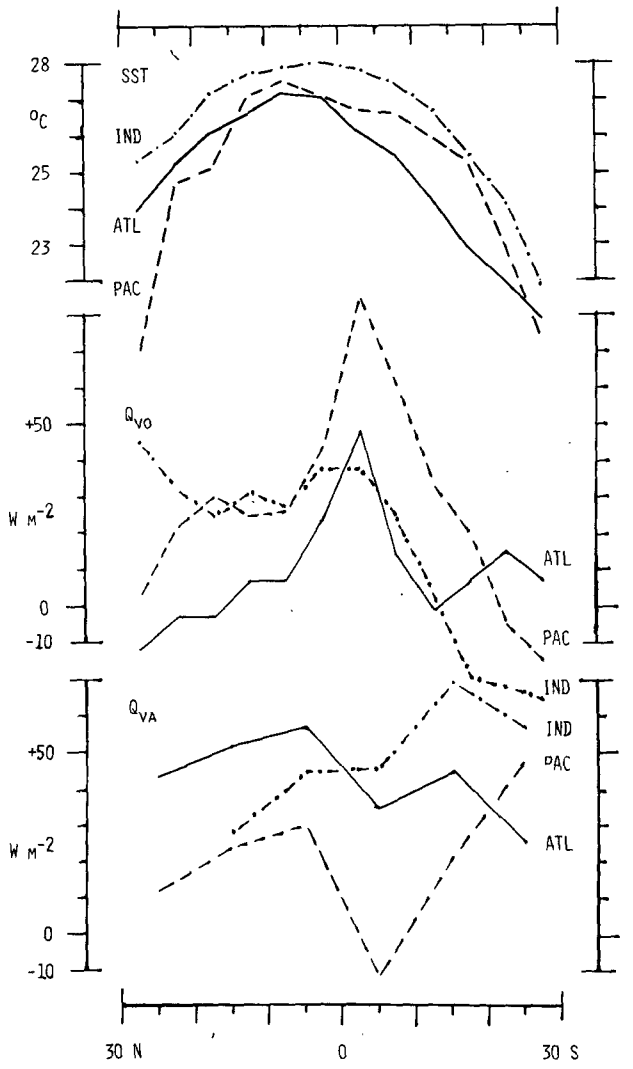

FIG. 6. Annual mean meridional profiles of sea surface temperature T(°C), and of divergence of heat transport (W m^{-2}) within ocean Q_{vo}, and atmosphere Q_{va}. Atlantic solid, Pacific broken and Indian Ocean dash-dotted lines [source: Figs. 4a and 4b for Q_{vo} and Q_{va}; Hastenrath and Lamb (1977, 1979), and U.S. Navy Hydrographic Office (1944) for T].

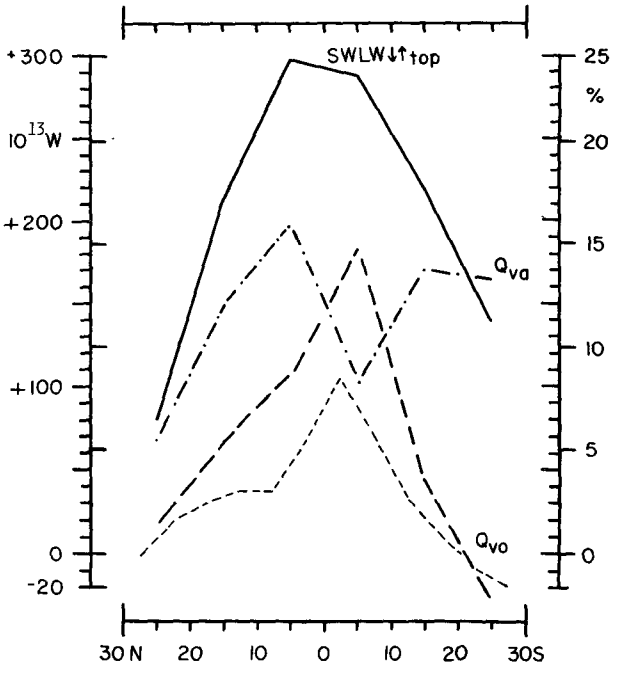

FIG. 7. Annual mean meridional profiles for the global tropics, heat budget terms for land and ocean combined. Net radiation at the top of the atmosphere, SWLW$\Uparrow_{top}$, solid; heat export within the atmosphere, Q_{va}, dash-dotted; heat export within the ocean, Q_{vo}, broken; thin dashed line refers to 5° band and thick line to 10° band. Scales are in 10^{13} W and in percent of SWLW$\Uparrow_{top}$ for 30°N–30°S = 1238 × 10^{13} W (source: Tables 1, 2 and Fig. 6).

the former the resolution corresponds to only 10° squares. This determines the 10° square resolution of the Q_{va} pattern. Calculations were performed for the 10° blocks lying within the areas identified in Fig. 1 by cross-hatching. Fig. 4c shows atmospheric heat export for most of the low latitudes, but especially the southern Indian Ocean, the South Atlantic, the western North Atlantic and equatorial Africa. Heat import is indicated for the deserts of northern Africa, the cold water regions along the coasts of eastern Africa and Arabia, and particularly a band immediately to the south of the equator in the eastern and central Pacific. Similarly, the atmospheric heat export is comparatively small to the south of the Atlantic equator. The latter features are a direct

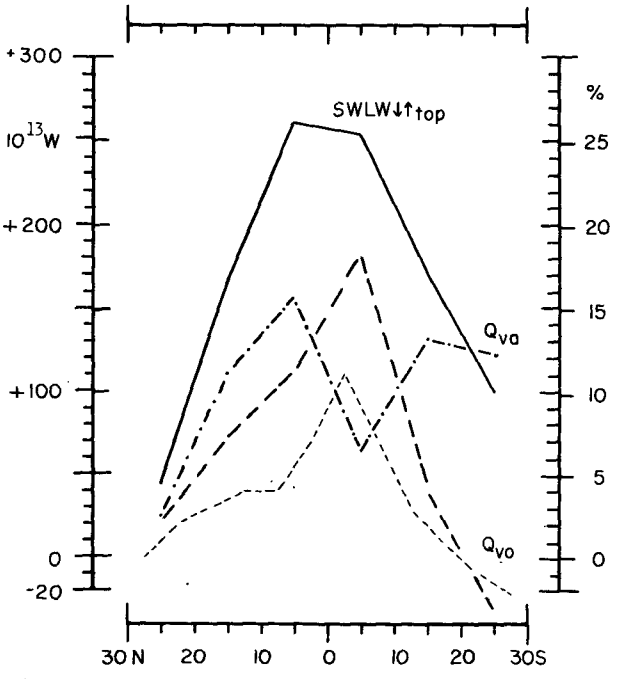

FIG. 8. As in Fig. 7 but with SWLW$\Uparrow_{top}$ for 30°N–30°S = 1008 × 10^{13} W = 100%.

TABLE 2. Total area of latitude zones and percentage contribution of various oceans and continents (in part from List, 1968, Table 164).

Latitude zone	Total area (10^9 m^2)	Pacific	Atlantic	Indian	Americas	Africa	South Asia	Australia
30–25°N	19 699	35	23	1	5	13	23	0
25–20°N	20 499	37	22	6	3	15	17	0
20–15°N	21 145	39	20	13	3	15	10	0
15–10°N	21 663	42	18	17	2	16	5	0
10–5°N	21 960	44	13	18	6	17	2	0
5–0°N	22 124	45	17	17	8	10	3	0
0–5°S	22 124	42	15	19	11	8	5	0
5–10°S	21 960	42	13	22	12	8	3	0
10–15°S	21 633	44	14	22	11	8	0	1
15–20°S	21 145	41	14	21	9	9	0	6
20–25°S	20 499	39	16	21	7	7	0	10
25–30°S	19 699	38	18	23	6	4	0	11

result of the maxima of oceanic heat export Q_{vo} to the south of the Pacific and Atlantic equator and off the Somali-Arabian coasts, and the rather uniform horizontal pattern of net radiation at the top of the atmosphere SWLW$\uparrow\downarrow_{top}$.

Mean meridional profiles of Q_{va} are shown in Fig. 6 for the three oceans and in Table 1 for the four continents. The profiles for the three individual oceans illustrate the existence of a minimum of Q_{va} to the south of the equator in the Atlantic and Pacific, and its absence in the Indian Ocean. This is a direct consequence of the meridional profiles of Q_{vo} in the three oceans; the cold water conditions during the northern summer monsoon season contribute toward the large Q_{vo} in the northern Indian Ocean. For all oceans combined (Figs. 5, 7 and 8), the prominent maximum of oceanic heat export Q_{vo} immediately to the south of the equator along with the more nearly hemispherically symmetric pattern of net radiation at the top of the atmosphere SWLW$\uparrow\downarrow_{top}$ result in a conspicuous minimum of atmospheric heat export Q_{va} in a latitude band immediately to the south of the equator. This feature is strongly dictated by the patterns of the Pacific and Atlantic Oceans.

It is recalled that net atmospheric heat export Q_{va} typically results from import of latent heat Lq in the lower, and export of geopotential energy and sensible heat ($gz + c_pT$) in the upper troposphere, and vice versa (Riehl and Malkus, 1958; Hastenrath, 1966; Hastenrath and Lamb, 1980). This is related to the characteristic vertical distribution of the various atmospheric energy forms and the intensity and direction of the vertical circulation. While these processes within the atmosphere are not explicitly assessed, the values of Q_{va} arrived at here as residual stand in their own right.

In accordance with the available satellite information, heat budget terms shown in Table 1 and Figs. 4–6 were evaluated by Marsden squares contained within the areas identified in Fig. 1 by cross-hatching. The areas shown in Fig. 1 are regarded as representative samples of the three tropical oceans and four continents. The areal breakdown in Table 2 allows a weighting according to the various large land and sea areas. On this basis, the absolute magnitude of heat budget terms for the tropics as a whole was estimated and plotted in Fig. 7 in profile form. In addition to absolute energy quantities by latitude belts, terms are also expressed as percentages of the total annual radiative heat gain at the top of the atmosphere in the tropics, 30°N–30°S. Fig. 7 is complemented by Table 3. Consistent with Fig. 6, the profiles in Fig. 7 and Table 3 show approximate hemispheric symmetry for SWLW$\uparrow\downarrow_{top}$, with the maximum to the north of the equator. The maximum of oceanic heat export Q_{vo} immediately to the south of the equator is concomitant with a conspicuous minimum of atmospheric heat export Q_{va}. The largest amounts of atmospheric heat export Q_{va} are found in the band to the north of the equator. However, despite the comparatively large share of land

TABLE 3. Annual heat budget pattern for the global tropics, land and ocean combined. Values are expressed as a percentage of SWLW$\uparrow\downarrow_{top}$ for 30°N–30°S = 1238 × 10^{13} W. Symbols as for Fig. 2.

Latitude zone	Q_{vo}	SWLW$\uparrow\downarrow_{top}$	Q_{va}	
30–25°N	0	7	+5	30–20°N
25–20°N	+2			
20–15°N	+2	17	+12	20–10°N
15–10°N	+3			
10–5°N	+3	24	+16	10–0°N
5–0°N	+6			
0–5°S	+9	23	+8	0–10°S
5–10°S	+6			
10–15°S	+3	18	+14	10–20°S
15–20°S	+1			
20–25°S	−1	11	+13	20–30°S
25–30°S	−2			
30°N–30°S	+32	100	+68	

in the total surface of the band 0–10°N, the entire atmospheric heat export from this belt is little larger than the oceanic heat export Q_{vo} from the band 0–10°S. In fact, the oceanic heat export effected by the band 0–5°S is more substantial by comparison.

5. Relative role of oceanic versus atmospheric heat export

A separation of the total heat export from the tropics into the contributions by hydrosphere and atmosphere has been attempted by various recent studies (Vonder Haar and Oort, 1973; Oort and Vonder Haar, 1976; Hastenrath, 1977a,b; Hastenrath and Lamb, 1980). The results of such a procedure can be affected by the errors in the estimates of budget terms.

In contrast to the estimates of Q_{vo} and Q_{va}, an integral constraint is available for SWLW$\uparrow\downarrow_{top}$, in that an approximate balance can be postulated for the globe as a whole. Evaluation of the data by Vonder Haar and Ellis (1974) yields an annual figure of SWLW$\uparrow\downarrow_{top}$ for 30°N–30°S of $+1238 \times 10^{13}$ W (Table 3). No values are given for 80–90°S, but in view of the small area involved the contribution for this cap was approximated by the value for 80–90°N. On this basis, a value of -777×10^{13} W was obtained from Vonder Haar and Ellis (1974) for the annual net radiation at the top of the atmosphere SWLW$\uparrow\downarrow_{top}$ over the caps poleward of 30°N and 30°S. This corresponds to a global imbalance of $+461 \times 10^{13}$ W. Gruber (1978) obtained from a one year data set an imbalance of similar magnitude, but opposite sign, *viz.*, -500×10^{13} W. Such global integrals correspond to a systematic or unbalanced component of the random errors in SWLW$\uparrow\downarrow_{top}$ of the order of 10 W m^{-2}. These discrepancies may indicate the uncertainty in current satellite-derived estimates of planetary net radiation SWLW$\uparrow\downarrow_{top}$.

TABLE 4. Annual heat budget pattern for the global tropics, land and ocean combined. Values are expressed as a percentage of SWLW$\uparrow\downarrow_{top}$ for 30°N–30°S = 1008×10^{13} W. Symbols as for Fig. 2. (source: Table 3).

Latitude zone	Q_{vo}	SWLW$\uparrow\downarrow_{top}$	Q_{va}	
30–25°N	0	4	+2	30–20°N
25–20°N	+2			
20–15°N	+3	18	+11	20–10°N
15–10°N	+4			
10–5°N	+4	26	+15	10–0°N
5–0°N	+7			
0–5°S	+11	25	+7	0–10°S
5–10°S	+7			
10–15°S	+3	17	+13	10–20°S
15–20°S	+1			
20–25°S	−1	10	+13	20–30°S
25–30°S	−2			
30°N–30°S	+39	100	+61	

TABLE 5. Annual heat budget pattern for the global tropics, land and ocean combined. Values are expressed as a percentage of SWLW$\uparrow\downarrow_{top}$ for 30°N–30°S = 777×10^{13} W. Symbols as for Fig. 2. (source: Table 3).

Latitude zone	Q_{vo}	SWLW$\uparrow\downarrow_{top}$	Q_{va}	
30–25°N	0	7	+5	30–20°N
25–20°N	+2			
20–15°N	+4	17	+8	20–10°N
15–10°N	+5			
10–5°N	+5	24	+10	10–0°N
5–0°N	+9			
0–5°S	+14	23	−1	0–10°S
5–10°S	+9			
10–15°S	+4	18	+12	10–20°S
15–20°S	+1			
20–25°S	−1	11	+15	20–30°S
25–30°S	−3			
30°N–30°S	+51	100	+49	

Table 3 implies that the aforementioned errors in SWLW$\uparrow\downarrow_{top}$ are ascribed entirely to the caps poleward of 30°N and 30°S. This leads to a conservative estimate for the role of the oceans in the global heat budget. Accordingly, adjustments are of interest, as applied for Fig. 8 and Tables 4 and 5. Table 4 and Fig. 8 use a value of SWLW$\uparrow\downarrow_{top}$ for 30°N–30°S of $+1008 \times 10^{13}$ W, i.e., the global imbalance is distributed equally between the tropics and extratropics. In Table 5 it is assumed that the discrepancy is due entirely to errors within the tropical half of the earth, yielding a value of SWLW$\uparrow\downarrow_{top}$ = $+777 \times 10^{13}$ W for 30°N–30°S. Unless a case can be made for a marked latitude dependence of errors in SWLW$\uparrow\downarrow_{top}$, Fig. 8 and Table 4 may offer the most plausible picture.

6. Oceanic heat transport

The meridional transport of heat within the ocean can be obtained by assumption of an appropriate boundary condition and integration of Q_{vo} (Fig. 6) over latitude bands. Such curves have been constructed by Bryan (1962) and Emig (1967) for individual oceans on the basis of Budyko's (1963) atlas. Vonder Haar and Oort (1973) inferred the oceanic heat transport from satellite-derived net radiation at the top of the atmosphere, and calculations of the atmospheric heat transport. It is noted that in the latter study the oceanic heat transport is computed as the residual between two quantities which themselves are obtained as differences between large terms. Accordingly, sampling errors are sizeable.

In the present study, meridional heat transports within the individual oceans were calculated from the values of Q_{vo} for latitude bands between 30°N and 30°S (Fig. 6). For purposes of a northern boundary condition, Aagaard and Greisman's (1975)

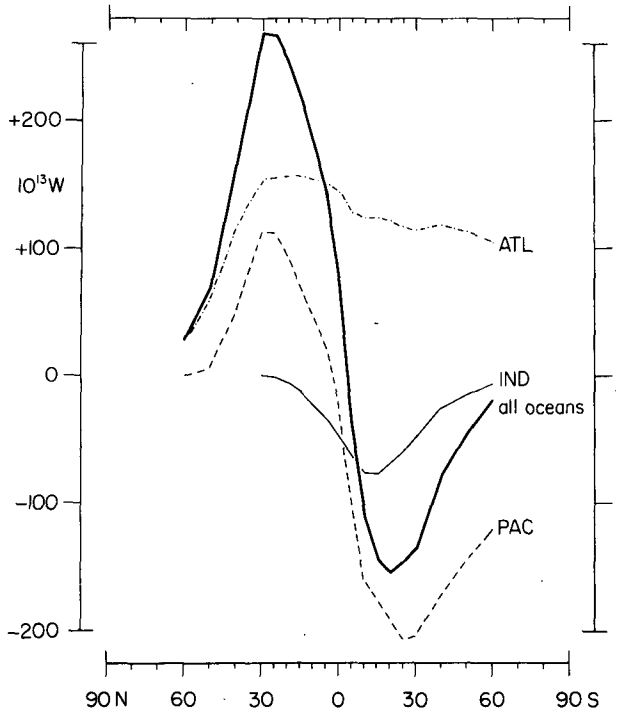

FIG. 9. Annual mean meridional heat transport within the oceans. Pacific broken, Atlantic dash-dotted, Indian Ocean thin solid, and all oceans combined heavy solid line. Northward transport positive, units in 10^{13} W [sources: Fig. 6 and Table 2 for 30°N–30°S; Budyko (1963) for 30–66°N and 30–60°S; and Aagaard and Greisman (1975) for 66–90°N].

estimates for the Arctic Basin were used. Furthermore, Budyko's (1963) atlas was available for the zones 66–30°N and 30–60°S. Integration proceeded from north to south. In the high latitudes of the Southern Hemisphere, 70°W, 20°E and 120°E were used as divisions between the Pacific, Atlantic and Indian Oceans. Emig (1967) chose similar boundaries. Results are presented in profile form in Fig. 9, and further illustrated in the map scheme in Fig. 10.

The characteristics of meridional heat transport differ remarkably for the three oceans. In the Pacific sector, heat exchange across the Bering Straits is small (Aagaard and Greisman, 1975), as is the poleward transport around 60°N. The largest values are indicated for 30°N, and transport changes to southward somewhat north of the equator. Thus the large heat gain in the band 0–5°S (Figs. 6 and 10) is carried southward in its entirety. The largest southward transport is found near 20°S. By virtue of its large area, the Pacific dominates the pattern for all oceans combined.

In the Atlantic, the oceanic heat transport is directed northward, from 60°S all the way to the arctic. The large oceanic heat surplus in the band 0–5°S (Figs. 6 and 10) reflects itself in a marked increase of northward heat transport. Values remain high throughout the Northern Hemisphere tropics, reach a maximum at 15°N, and drop off sharply poleward of 30°N. The prominent transport char-

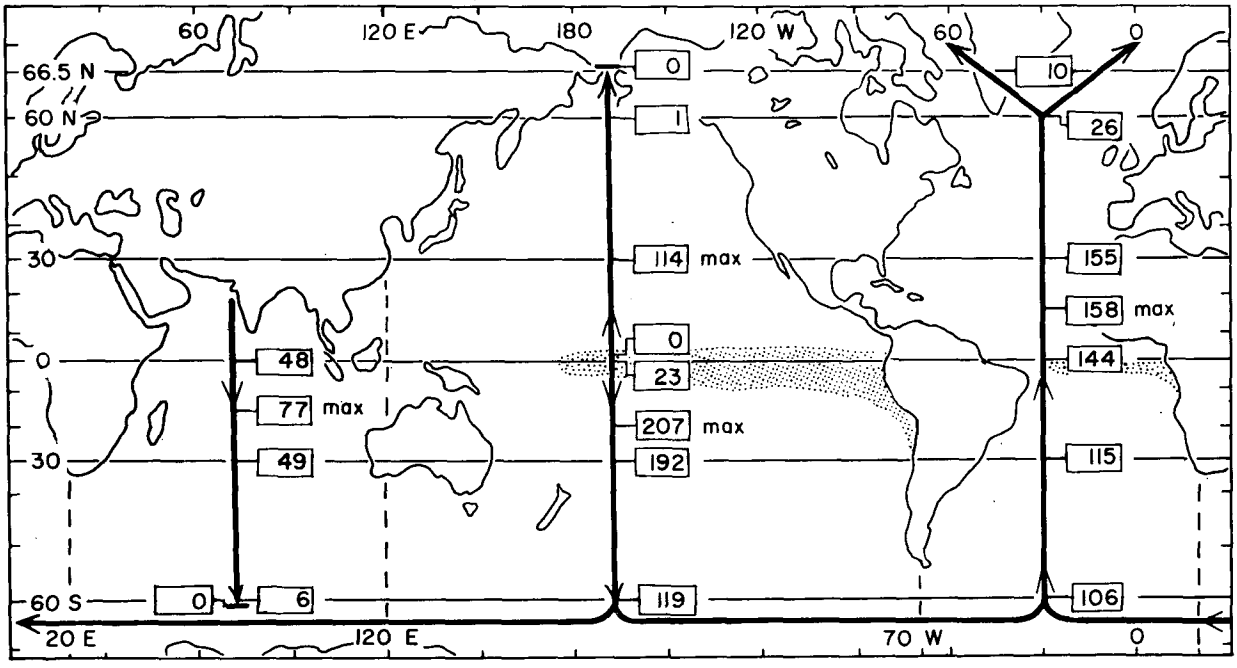

FIG. 10. Map scheme of annual mean meridional heat transport within the oceans (from Fig. 9). Heavy cross bar denotes latitude of zero, and max that of maximum meridional transport, with numbers indicating amounts in units of 10^{13} W. Stippling marks areas with $Q_{vo} < +50$ W m^{-2} in Fig. 4b, and broken lines show the meridians used as boundaries between oceans in the high southern latitudes.

acteristics in the Atlantic, as compared to the Pacific, are related to the open communication with the arctic basin and the concomitant large heat deficit in high northern latitudes, and to the large oceanic heat gain in the Southern Hemisphere tropics associated with the comparatively low sea surface temperature (Figs. 6 and 2).

As a result of the continent configuration, meridional heat transport in the Indian Ocean is directed southward, with a maximum around 10–15°S and a decrease to near nil at 60°S. Heat deficits in the higher southern latitudes of the Indian and Atlantic Ocean sectors must be compensated by contributions from the Pacific domain. Furthermore, heat input from the Pacific helps balance the heat budget of the Atlantic sector at large.

For all oceans combined, maximum northward and southward heat transport are found at 30°N and 20°S, respectively, and a net northward transport is indicated at the equator. A closure of Fig. 10 is desirable in terms of a comparison with the heat budget of the Antarctic Ocean poleward of 60°S. From Zillman's [1972, Fig. 1.10(e), p. 114] map of annual $(Q_v + Q_t)_o$ the required poleward directed oceanic heat transport across 60°S can be estimated to be of the order of $10-20 \times 10^{13}$ W. In the light of the coarse spatial resolution of Zillman's map this compares favorably with the value of 13×10^{13} W resulting from Figs. 9 and 10.

For the World Ocean as a whole, Emig (1967) found similar latitudes of the extrema as in Fig. 6, but smaller and larger poleward transports in the Northern and Southern Hemispheres, respectively. Accordingly, her tabulations show a southward rather than a northward directed net transport across the equator. Vonder Haar and Oort (1973) computed a maximum poleward transport around 20°N, and a net northward transport across the equator. Their poleward heat flux maximum is considerably larger than arrived at in the present study. They concluded that the hydrosphere performed 74 and 47% of the total poleward heat transport at latitudes 20 and 30°N, respectively. The corresponding figures in Oort and Vonder Haar's (1976) study are 73 and 42%. The atlas available to Emig (1967) for the tropics is inferior to the present data sources. Vonder Haar and Oort (1973) used a novel approach in that they calculated Q_{vo} as a residual in Eq. (1).

The poleward heat transport for all oceans combined (Fig. 9) is compared in Fig. 11 with the total transport in the ocean-atmosphere system. The latter parameter is plotted from Gruber (1978), since he established a zero balance adjustment for the globe as a whole. The meridional heat transport within the atmosphere is entered as the difference between the former two curves.

Fig. 11 illustrates the relative importance of oceanic heat transports in the tropics, especially of the Northern Hemisphere, accounting for 55 and 53% of the total transport at 20 and 30°N, respectively. By comparison, the maximum southward oceanic transport at 20°S amounts to only 35% of the total transport. Meridional heat transport within the atmosphere is largest in midlatitudes where it indeed effects the bulk of the total transport for the ocean-atmosphere system. It is recalled that a substantial portion of the poleward heat transport in the atmosphere of the Northern Hemisphere extratropics takes place in the form of latent heat (Oort and Rasmusson, 1971; Rosen *et al.*, 1979).

Estimates of Oort and Vonder Haar (1976) are also entered in Fig. 11 for comparison. Their figures for the combined ocean-atmosphere system are somewhat smaller than Gruber's (1978) values from a different satellite and a different period. Their maximum oceanic heat transport is larger and located at a lower latitude. Using the larger values of Gruber, their residual method would not lead to a better overall agreement with the present curve of oceanic transport since discrepancies at the latitude band of largest transport are larger than 20%. Regarding the atmospheric transport, the present study would agree even more closely with the figures of Oort and Vonder Haar, if their smaller values for the combined ocean-atmosphere system were used. In fact, in the latitude band of largest atmospheric transport the present values and those of Oort and Vonder Haar would differ by less than 10%.

7. On error estimates

Error estimates are essential in budget studies, but they are unsatisfactory at present. As a rule, shortcomings related to temporal and spatial sampling and instrumental inaccuracy, and random versus systematic components, are not readily separated.

For the satellite-derived net radiation at the top of the atmosphere, Vonder Haar and Oort (1973) suggest a "probable bias" error of latitude means not exceeding 7 W m^{-2}. Ellis *et al.* (1978) propose a "total uncertainty" in the global mean of net radiation at the top of the atmosphere of $\sim$10 W m^{-2}. This figure implies errors of appreciably larger magnitude for, say, individual 10° square areas. As pointed out in Section 5, the imbalances in the global mean of annual net radiation at the top of the atmosphere resulting from the studies of Vonder Haar and Ellis (1974) and Gruber (1978) are of comparable magnitude, namely around 10 W m^{-2} but opposite sign. In the Nimbus-6 ERB Experiment, Jacobowitz *et al.* (1979) obtained an imbalance of less than 6 W m^{-2}.

The apparent interannual variability of satellite-derived net radiation at the top of the atmosphere noted by Vonder Haar and Oort (1973) would correspond to a probable error of $\sim$6 W m^{-2} for the belt

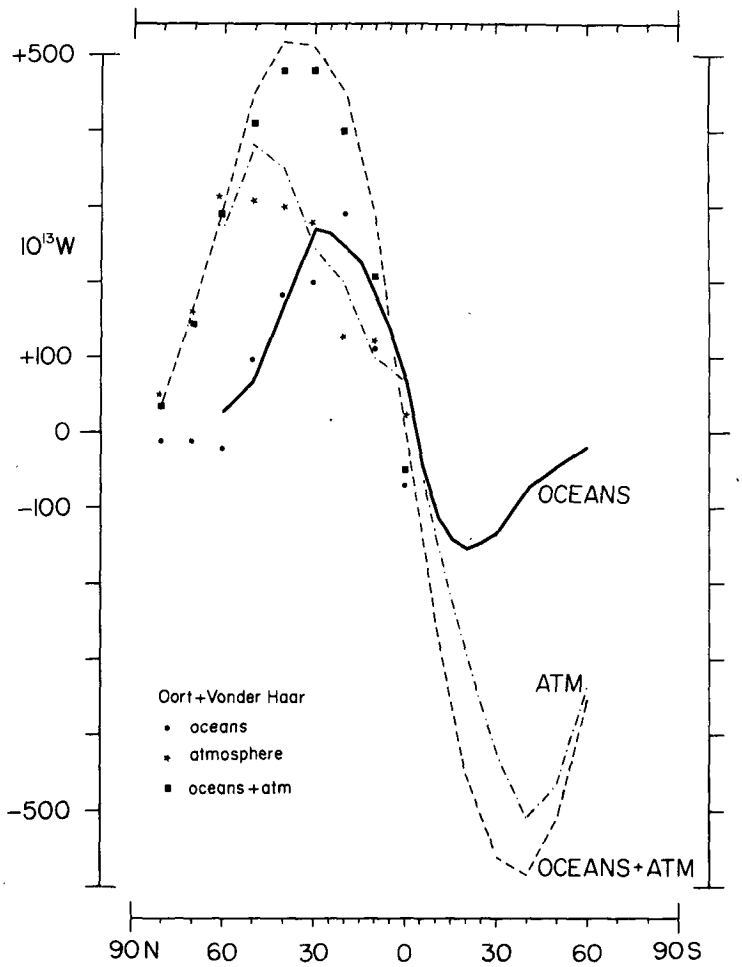

FIG. 11. Annual mean meridional heat transport within the atmosphere-ocean system broken (source: Gruber, 1978), within the oceans solid (from Fig. 9), and within the atmosphere (residual) dash-dotted line. Dots, stars and squares show values of Oort and Vonder Haar (1976) for Northern Hemisphere ocean, atmosphere, and ocean plus atmosphere combined, respectively. Northward transport positive.

0–30°N. Similar figures are given in Oort and Vonder Haar (1976). Flanders and Smith (1975) report a figure of 7 W m^{-2} for the difference in global mean of net radiation at the top of the atmosphere during May 1970 versus 1971, but obtained from two different satellite systems. The interannual variability apparent from satellite data presumably differs from the "true" variability of global mean net radiation at the top of the atmosphere, which is not known, but is expected to be small. Different satellite sensing systems are presumably fraught with different random and systematic errors.

According to the classical rule of *random* error propagation an error of 10 W m^{-2} in the global mean would correspond to errors of 20 and 35 W m^{-2} for the bands 0–30°N or S, and a 10° latitude band of the tropics, respectively. However, a certain portion of the aforementioned error of 10 W m^{-2} is likely to be systematic, and its relative contribution is not known. Only a fraction of this imbalance is likely to stem from a "true" interannual variability. Any adjustment aimed at achieving a zero global mean of radiation at the top of the atmosphere, as exemplified in Section 5, Tables 3–5 and Figs. 7 and 8, will still lead to errors that are at least as large as the "true" interannual variability. In terms of the measurement, $SWLW\Uparrow\Downarrow_{top}$ is a small difference between the downward and upward directed shortwave and the upward directed longwave radiation. Accordingly, efforts at substantially improving over a 6–10 W m^{-2} error in $SWLW\Uparrow\Downarrow_{top}$ may involve a formidable task in the determination of component fluxes. This brief review of evidence cautions against optimistic estimates of errors in the presently available satellite-derived net radiation at the top of the atmosphere.

Errors in atmospheric transport related to interannual variability (Oort, 1977) have been estimated

by Vonder Haar and Oort (1973) and Oort and Vonder Haar (1976). These figures are small; in fact, the corresponding probable error in the annual atmospheric heat export Q_{va} from the zone 0–30°N would amount to only ~2 W m^{-2}. It is also appreciated that appropriate adjustments have ensured internal consistency in the MIT General Circulation Project data. However, the lack of actual upper air observations in large areas of the tropics (Oort, 1978) cannot be made up by analysis techniques. Among the most critical data-sparse areas are the vast expanses of the Pacific and the realm of jetlike wind concentrations over the western Indian Ocean. Furthermore, an evaluation of the annual mean meridional energy transports tabulated by Oort and Rasmusson (1971) according to energy components, layers and latitude belts, illustrates that the net export results as a small difference between large terms. It is here proposed that the error in the net atmospheric energy export Q_{va} from the belt 0–30°N, as related to the effect of small differences, may well be of the order of 5 W m^{-2}. More importantly, internal data consistency does not preclude sizeable systematic errors in Q_{va}, the magnitude of which is not known.

The error in Q_{vo} in the sense of a "total uncertainty" has been estimated to be of the order of 20–30 W m^{-2} (Hastenrath, 1977a). A sizeable portion of this figure accounts for a possible systematic error in Q_{va}, as it would result from systematic uncertainties primarily in the net longwave radiation. Truly random errors would be of little consequence by comparison.

Values in Figs. 9–11 shall now be compared against this background. A systematic error of 10 W m^{-2} in Q_{vo} would lead to an error of the order of 100×10^{13} W in the oceanic heat transport around 30°N. Similar considerations apply to $\mathrm{SWLW}\uparrow\downarrow_{top}$. It is suggested that errors in the oceanic transport calculated by Vonder Haar and Oort (1973) as a residual from satellite-derived net radiation at the top of the atmosphere and computations of the atmospheric heat budget are at least of comparable magnitude. Within these broad error bounds the much larger oceanic transport estimates by Vonder Haar and Oort (1973) and Oort and Vonder Haar (1976) must be considered as compatible with the present ones (Figs. 9–11).

8. Conclusions

Classical concepts of the global heat budget have emphasized the role of upper tropospheric export from the realm of the quasi-planetary near-equatorial band of maximum convergence (ITCZ). A "hot-tower" mechanism of undiluted cumulonimbus cores was invoked to carry heat from the surface layer through the mid-tropospheric energy minimum into the upper troposphere, from where it would be exported laterally to higher latitudes (Riehl and Malkus, 1958). The present analysis invites a reappraisal of the relative role of the tropical atmosphere and hydrosphere in the heat budget of the globe.

Tables 1–5 and Figs. 4–11 illustrate the relative importance of the ocean in disposing of the heat surplus from the tropics. The radiative heat gain at the top of the atmosphere over land is rather smaller than over sea, and is in its totality disposed of within the atmospheric column. For the tropical oceans, the ratio of hydrospheric to total heat export follows a pattern similar to Q_{vo}, because of the comparatively modest spatial variation of net radiation at the top of the atmosphere.

The partitioning of total heat export into the atmospheric and hydrospheric contributions requires satellite-derived estimates of planetary net radiation that are consistent with a balance for the globe as a whole. Fig. 8 and Table 4 adjust imbalances equally between the tropics (30°N–30°S) and the extratropics, yielding $1008 \times 10_{13}$ W (=100 units) for the total annual heat gain $\mathrm{SWLW}\uparrow\downarrow_{top}$ in the belt 30°N–30°S.

Of the total annual heat gain in the belt 30°N–30°S, only 20 units are exported by the atmosphere over land (Tables 1, 2, 4 and Fig. 8); the same data show that for the tropical oceans at large, exports by atmosphere and water body amount to 41 and 39 units.

The planetary cloud-band (ITCZ) is confined throughout the year to the latitude band 0–10°N, except for longitudes 50–100°E of the Indian Ocean sector, where the maximum cloud zone is displaced farther north during northern summer (Fig. 2). The annual atmospheric heat export Q_{va} from this latitude zone amounts to only 13 units (Fig. 8, Table 4). If the band 10–20°N is substituted for the longitudes 50–100°E, a substantially smaller figure is obtained (Fig. 4c, Table 2). By comparison, the oceanic export Q_{vo} from the zone 0–10°S is 18 units, and 11 of these units stem from the belt 0–5°S alone. In fact in this strip immediately to the south of the equator some 90% of the net radiation at the top of the atmosphere is disposed of by export within the oceanic water body Q_{vo}. Viewed in perspective, heat export Q_{va} from the realm of the ITCZ by atmospheric motions plays a modest *relative* role, while oceanic export Q_{vo} from the cold water zones immediately to the south of the equator in the eastern Atlantic and eastern and central Pacific is an at least comparably important factor in the heat export to the extratropics. In *absolute* terms, however, the atmospheric heat export Q_{va} from the band 0–10°N as given in Fig. 8 and Table 4 is about twice as large as the classical estimates (Riehl and Malkus, 1958) that minimize the role of the oceans but use the much smaller values of $\mathrm{SWLW}\uparrow\downarrow_{top}$ calculated by London (1957) as input. Thus Fig. 8 and Table 4 show for the band 0–10°N values of $\mathrm{SWLW}\uparrow\downarrow_{top} = 26$ and $Q_{va} = 15$, as compared to London's (1957) annual $\mathrm{SWLW}\uparrow\downarrow_{top} = 8$ units, all in 10^{14} W.

Integration of oceanic heat export indicates poleward heat transport from the tropics into either hemisphere in the Pacific; a northward directed transport from high southern latitudes all the way to the Arctic in the Atlantic; and southward transport in the Indian Ocean. Oceanic heat surplus in the Pacific compensates deficits in the higher southern latitudes of the Atlantic and Indian Ocean sectors, as well as in the Atlantic at large. For all oceans combined, heat transport is largest around 30°N and 20°S, where it accounts for 53 and 35% of the total meridional transport in the ocean-atmosphere system. For the globe as a whole, the sign of the net cross-equatorial oceanic heat transport is uncertain, in terms of the error limits proposed here. However, a northward-directed heat transport from the Southern to the Northern Hemisphere domain of the World Ocean of similar magnitude as shown in Figs. 9 and 10 is also inferred from independent considerations (H. Lettau, personal communication, 1979). Atmospheric transport is largest, and effects the bulk of the total transport in midlatitudes.

The relative partitioning proposed here is contingent upon the representativeness of satellite-measured net radiation at the top of the atmosphere and the computation of the oceanic heat budget. Appreciably different estimates of $SWLW\Uparrow\Downarrow_{top}$, Q_{vo} and Q_{va} must be considered as compatible within the broad error limits indicated for all three terms.

Acknowledgments. This study was supported through Office of Naval Research–Atmospheric Sciences Program Contract N00014-78-C0190 and National Science Foundation–Climate Dynamics Research Program Grants and ATM76-09784 and ATM79-11131. I thank Peter J. Lamb (CIMAS, Miami), William L. Smith (SSEC, Madison) and Abraham H. Oort (GFDL, Princeton) for discussions and comments on a draft version of this paper.

REFERENCES

Aagaard, K., and P. Greisman, 1975: Towards new mass and heat budgets for the Arctic Basin. *J. Geophys. Res.*, **80,** 3821–3827.

Atkinson, G. D., and J. Sadler, 1970: Mean-cloudiness and gradient-level-wind charts over the tropics. U.S. Air Force, AWS Tech. Rep. No. 215, 48 pp.

Bryan, K., 1962: Measurements of meridional heat transport by ocean currents. *J. Geophys. Res.*, **67,** 3403–3413.

Budyko, M. I., 1963: *Atlas of the Heat Balance of the Earth.* Kartfabrika Gosgeoltehizdata, Leningrad, 75 pp.

Ellis, J. S.; Th. H. Vonder Haar, S. Levitus and A. H. Oort, 1978: The annual variation of the global heat balance of the Earth. *J. Geophys. Res.*, **83,** 1958–1962.

Emig, M., 1967: Heat transport by ocean currents. *J. Geophys. Res.*, **72,** 2519–2529.

Flanders, D. H., and W. L. Smith, 1975: Radiation budget data from the meteorological satellites ITOS 1 and NOAA 1. NOAA Tech. Memo. NESS 72, Washington, DC, 20 pp.

Gruber, A., 1978: Determination of the earth-atmosphere radiation budget from NOAA satellite data. NOAA Tech. Rep. NESS 76, Washington, DC, 28 pp.

Hastenrath, S., 1966: On general circulation and energy budget in the area of the Central American seas. *J. Atmos. Sci.*, **23,** 694–711.

——, 1977a: Relative role of atmosphere and ocean in the global heat budget: Tropical Atlantic and eastern Pacific. *Quart. J. Roy. Meteor. Soc.*, **103,** 519–526.

——, 1977b: Atmospheric and oceanic heat export in the tropical Pacific. *J. Meteor. Soc. Japan*, **55,** 494–497.

——, 1978: Hemispheric asymmetry of the oceanic heat budget in the equatorial Atlantic and Eastern Pacific. *Tellus*, **29,** 523–529.

——, and P. Lamb, 1977: *Climatic Atlas of the Tropical Atlantic and Eastern Pacific Oceans.* University of Wisconsin Press, 105 pp.

——, and ——, 1978a: On the dynamics and climatology of surface flow over the equatorial oceans. *Tellus*, **30,** 436–448.

——, and ——, 1978b: *Heat Budget Atlas of the Tropical Atlantic and Eastern Pacific Oceans.* University of Wisconsin Press, 104 pp.

——, and ——, 1979: *Climatic Atlas of the Indian Ocean. Part 1. Surface Circulation and Climate. Part 2. The Oceanic Heat Budget.* University of Wisconsin Press, 104 pp.

——, and ——, 1980: On the heat budget of hydrosphere and atmosphere in the Indian Ocean. *J. Phys. Oceanogr.*, **10** (in press).

Jacobowitz, H., W. L. Smith, H. B. Howell, F. W. Nagle and J. R. Hickey, 1979: The first eighteen months of planetary radiation budget measurements from the Nimbus 6 ERB experiment. *J. Atmos. Sci.*, **36,** 501–507.

List, R. J., 1968: *Smithsonian Meteorological Tables*, 6th ed. Smithsonian Institution Press, Washington, DC, 527 pp.

London, J., 1957: A study of the atmospheric heat balance. Dept. Meteor. Oceanogr., New York University, Final Report No. 131, Contract AF 19(122)-165.

Oort, A. H., 1977: The interannual variability of atmospheric circulation statistics. NOAA Prof. Pap. No. 8, Rockville, MD, 76 pp.

——, 1978: Adequacy of the rawinsonde network for global circulation studies tested through numerical model input. *Mon. Wea. Rev.*, **106,** 174–195.

——, and E. M. Rasmusson, 1971: Atmospheric circulation statistics. NOAA Prof. Pap. No. 5, Rockville, MD, 323 pp.

——, and Th. H. Vonder Haar, 1976: On the observed annual cycle in the ocean-atmosphere heat balance over the Northern Hemisphere. *J. Phys. Oceanogr.*, **6,** 781–799.

Riehl, H., and J. S. Malkus, 1958: On the heat balance of the equatorial trough zone. *Geophysica*, **6,** 503–538.

Rosen, R. D., D. A. Salstein and J. P. Peixoto, 1979: Variability in the annual fields of large-scale atmospheric water vapor transport. *Mon. Wea. Rev.*, **107,** 26–37.

U.S. Navy Hydrographic Office, 1944; *World Atlas of Sea Surface Temperatures*, 2nd ed. H.O. Publ. No. 225, U.S. Govt. Printing Office, 49 pp.

Vonder Haar, Th. H., and A. H. Oort, 1973: New estimate of annual poleward energy transport by Northern Hemisphere oceans. *J. Phys. Oceanogr.*, **2,** 169–172.

——, and J. S. Ellis, 1974: Atlas of radiation budget measurements from satellites. Atmos. Sci. Pap. No. 231, Colorado State University, 180 pp.

Wyrtki, K., 1965: The average annual heat balance of the North Pacific Ocean and its relation to ocean circulation. *J. Geophys. Res.*, **70,** 4547–4559.

——, 1966: Seasonal variation of heat exchange and surface temperature in the North Pacific Ocean. Hawaii Institute of Geophysics, Rep. HIG-66-3, University of Hawaii, Honolulu.

Zillman, J. W., 1972: A study of some aspects of the radiation and heat budgets of the Southern Hemisphere oceans. Meteor. Stud. No. 26, Bureau of Meteorology, Melbourne, Australia, 562 pp.